ADVANCED HEALTHCARE MATERIALS
www.advhealthmat.de

Absorbable Thioether Grafted Hyaluronic Acid Nanofibrous Hydrogel for Synergistic Modulation of Inflammation Microenvironment to Accelerate Chronic Diabetic Wound Healing

Sha Liu, Qingfei Zhang, Jie Yu, Nannan Shao, Hongtong Lu, Jinshan Guo, Xuepeng Qiu, Dongfang Zhou, and Yubin Huang**

Current standard of care dressings are unsatisfactorily inefficacious for the treatment of chronic wounds. Chronic inflammation is the primary cause of the long-term incurable nature of chronic wounds. Herein, an absorbable nanofibrous hydrogel is developed for synergistic modulation of the inflammation microenvironment to accelerate chronic diabetic wound healing. The electrospun thioether grafted hyaluronic acid nanofibers (FHHA-S/Fe) are able to form a nanofibrous hydrogel in situ on the wound bed. This hydrogel degrades and is absorbed gradually within 3 days. The grafted thioethers on HHA can scavenge the reactive oxygen species quickly in the early inflammation phase to relieve the inflammation reactions. Additionally, the HHA itself is able to promote the transformation of the gathered M1 macrophages to the M2 phenotype, thus synergistically accelerating the wound healing phase transition from inflammation to proliferation and remodeling. On the chronic diabetic wound model, the average remaining wound area after FHHA-S/Fe treatment is much smaller than both that of FHHA/Fe without grafted thioethers and the control group, especially in the early wound healing stage. Therefore, this facile dressing strategy with intrinsic dual modulation mechanisms of the wound inflammation microenvironment may act as an effective and safe treatment strategy for chronic wound management.

1. Introduction

The population of adult diabetic patients has reached 450 million worldwide, almost 6% of the total population.[1] The risk of chronic diabetic ulcers in diabetic patients is 15%,[2] and the wounds have a poor prognosis, high recurrence rate, and often lead to amputation.[3] The healing of chronic cutaneous wounds in diabetes is an extremely complex process. The interactions of different cells contribute to all the stages of chronic wound healing, involving hemostasis, inhibition of inflammation, formation of granulation tissue, revascularization, re-epithelialization, and remodeling.[4] Chronic inflammation, which is mainly caused by the presence of a large number of reactive oxygen species (ROS), pro-inflammatory chemokines (secreted by inflammatory cells, such as M1 phenotype macrophages and neutrophils), and bacterial infection, is the primary reason for the long-term incurable nature of chronic wounds.[5] The chronic wounds tend to remain in the inflammation phase and rarely proceed to

Dr. S. Liu, Dr. Q. Zhang, Dr. J. Yu, Dr. N. Shao, Dr. H. Lu, Prof. D. Zhou, Prof. Y. Huang
State Key Laboratory of Polymer Physics and Chemistry
Changchun Institute of Applied Chemistry
Chinese Academy of Sciences
Changchun 130022, P. R. China
E-mail: east@ciac.ac.cn; ybhuang@ciac.ac.cn

Dr. S. Liu, Dr. Q. Zhang, Dr. J. Yu, Dr. N. Shao, Dr. H. Lu, Prof. X. Qiu, Prof. Y. Huang
University of Science and Technology of China
Hefei 230026, P. R. China

Dr. S. Liu, Prof. X. Qiu
Polymer Composites Engineering Laboratory
Changchun Institute of Applied Chemistry
Chinese Academy of Sciences
Changchun 130022, P. R. China

Prof. D. Zhou
School of Pharmaceutical Sciences
Southern Medical University
Guangzhou 510515, P. R. China

Prof. J. Guo
Department of Histology and Embryology
School of Basic Medical Sciences
Southern Medical University
Guangzhou 510515, P. R. China

The ORCID identification number(s) for the author(s) of this article can be found under https://doi.org/10.1002/adhm.202000198

DOI: 10.1002/adhm.202000198

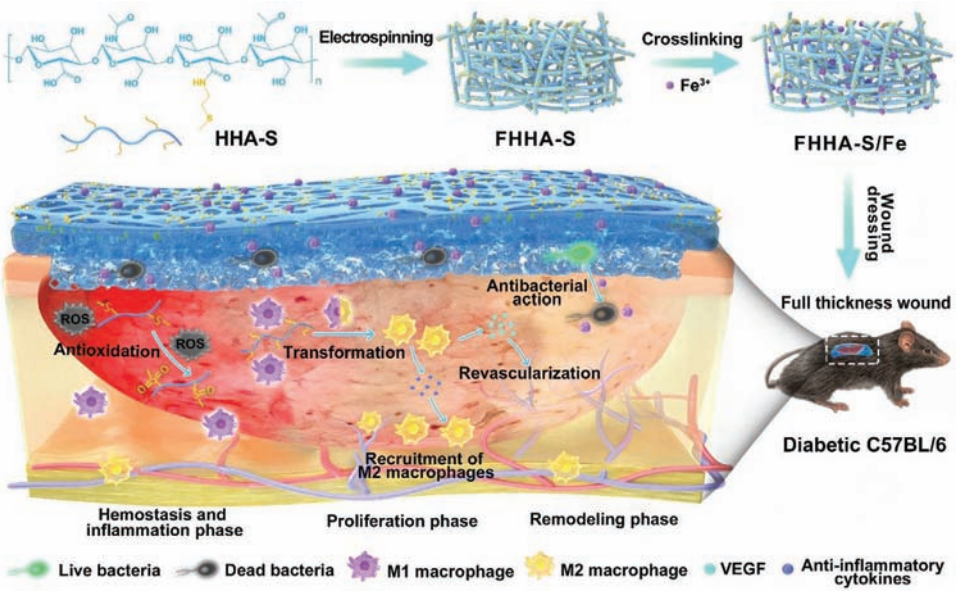

Scheme 1. Schematic illustration of the absorbable thioether grafted hyaluronic acid nanofibrous hydrogel for synergistic modulation of the inflammation microenvironment to accelerate chronic diabetic wound healing. Illustration of the preparation procedure of FHHA-S/Fe, dressing of FHHA-S/Fe on full-thickness wound model in diabetic C57BL/6 mouse, and the mechanism of FHHA-S/Fe for enhanced chronic wound healing effect.

the proliferation phase.[5d,6] Generally, the addition of antibiotics, anti-inflammatory drugs, and growth factors into the dressings is the main modality to eliminate chronic inflammation.[7] However, drug resistance, easy inactivation, and side effects of these bioactive agents cannot be ignored.[8] Recently, several systems have been developed by using dressing materials to modulate the wound inflammation microenvironment, including removal of ROS, adsorption of inflammatory factors, change of chemoattractant gradients, and regulation of the phenotype and number of immune cells.[5c,9] Although promising, these materials only focus on individual causes of chronic inflammation, of which the ensemble healing effect is often unsatisfactory. Thus, wound dressings with intrinsic synergistic modulation mechanisms of the wound inflammation microenvironment would have great potential for the treatment of chronic diabetic wounds.

Compared with traditional dry gauze dressings, new types of dressings based on films, hydrogels, hydrocolloids, foams, and nanofibers have been developed, which better promote wound healing.[7a,10] Nevertheless, almost none of these wound dressings are completely biodegradable or absorbable. In clinical practice, dressings need to be changed frequently for diabetic chronic wounds, with a frequency of once every two to three days for superficial skin wounds and once per day for deeper wounds with more exudate. Frequent dressing changes not only increase the cost and difficulty of patient care, but also often cause secondary injury to the wound. Recently, completely absorbable wound dressings were reported which eliminate the need to change dressings. However, the absorption time of these wound dressings was generally more than 10 days, which cannot meet the frequency required for dressing changes in chronic diabetic wounds.[11] Electrospun nanofibers prepared from hydrophilic polymers, after being properly crosslinked, can absorb wound exudate to form nanofibrous hydrogels. These nanofibrous hydrogels can keep the moist environment of the wound bed and maintain the advantages of cell infiltration and cell-material interactions from nanofibers.[12] Therefore, absorbable nanofibrous hydrogels that match the frequency of dressing change would show great efficacy in diabetic chronic wounds.

As one of the main components of extracellular matrix, hyaluronic acid (HA) has excellent biocompatibility. Moreover, high molecular weight HA (HHA) can promote the transformation of macrophages from a pro-inflammatory M1 to a reparative M2 phenotype.[13] M2 phenotype macrophages can greatly reduce inflammation and promote proliferation by releasing anti-inflammatory cytokines and growth factors.[5d,9c,14] Herein, to address the clinical needs, we designed an absorbable, thioether grafted HHA-based nanofibrous hydrogel system for synergistic modulation of the inflammation microenvironment to accelerate chronic diabetic wound healing (**Scheme 1**). Thioether grafted HHA (HHA-S) was electrospun into HHA-S nanofibers (FHHA-S), which were further crosslinked by Fe^{3+} to construct crosslinked nanofibers (FHHA-S/Fe). Iron is an essential trace element in the human body and Fe^{3+} shows broad-spectrum antibacterial action making it an excellent choice for a biocompatible cross-linking agent.[15] After being applied on the chronic diabetic wound bed, FHHA-S/Fe would form a nanofibrous hydrogel after absorbing wound exudate, which would be completely absorbed in a time frame matching typical dressing changes. The composition of the nanofibrous hydrogel provides many additional benefits along with its biodegradable and absorbable nature. The grafted thioethers on HHA would scavenge the ROS quickly in the early inflammation phase to reduce inflammation reactions. Additionally, the HHA itself would promote the transformation of the gathered M1 macrophages to an M2 phenotype, thus accelerating the wound healing phase transition from inflammation to proliferation and remodeling. Hence, the absorbable FHHA-S/Fe nanofibrous hydrogel, with its synergistic modulation mechanisms of the inflammation

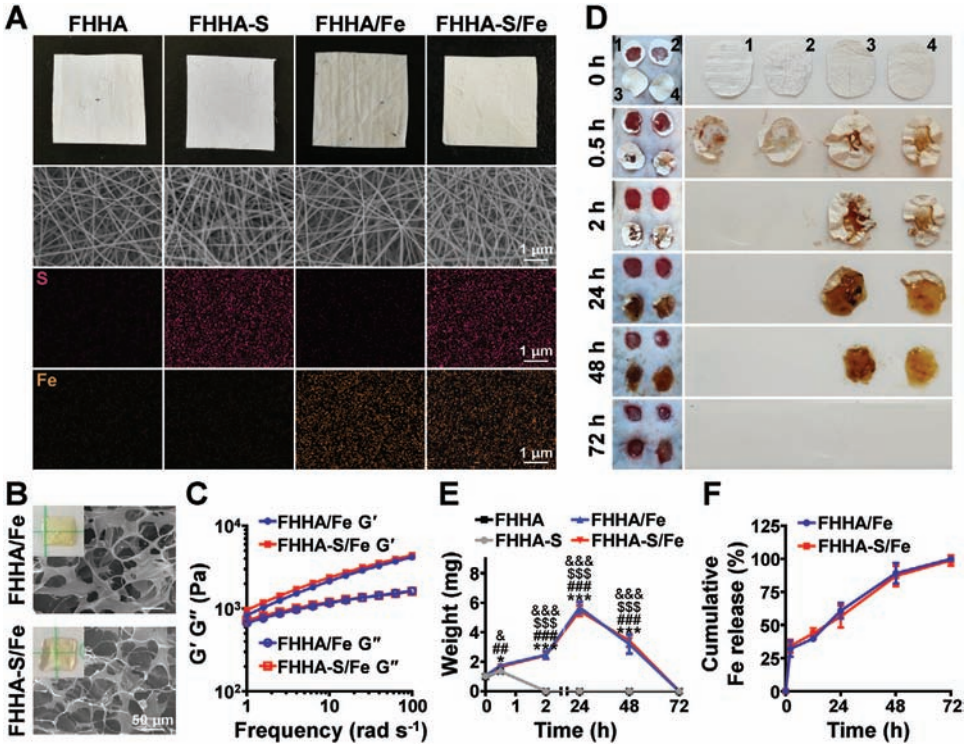

Figure 1. FHHA-S/Fe formed absorbable nanofibrous hydrogels after absorbing saline or wound exudate. A) Photographs, SEM images, and elemental mappings (S and Fe) of different nanofibers. B) Photographs of FHHA/Fe and FHHA-S/Fe after absorbing saline, and SEM images of nanofibrous hydrogels. C) The storage modulus (G') and loss modulus (G'') of FHHA/Fe and FHHA-S/Fe nanofibrous hydrogels. D) Photographs of different nanofibers (1 FHHA, 2 FHHA-S, 3 FHHA/Fe, and 4 FHHA-S/Fe) applied to and taken from the wound at indicated time. E) The weight of different nanofibers after dressing on the wound bed in vivo at indicated time. $^{*}p < 0.05$, $^{***}p < 0.001$ FHHA/Fe versus FHHA. $^{\#\#}p < 0.01$, $^{\#\#\#}p < 0.001$ FHHA/Fe versus FHHA-S. $^{\$\$\$}p < 0.001$ FHHA-S/Fe versus FHHA. $^{\&}p < 0.05$, $^{\&\&\&}p < 0.001$ FHHA-S/Fe versus FHHA-S. $n = 3$. F) Release profiles of Fe from FHHA/Fe and FHHA-S/Fe at pH = 7.4. $n = 3$.

microenvironment, is expected to exhibit an excellent healing effect for chronic diabetic wounds without adding any other active ingredients and while avoiding secondary injury.

2. Results and Discussion

2.1. FHHA-S/Fe Formed Absorbable Nanofibrous Hydrogels after Absorbing Saline or Wound Exudate

To construct the absorbable FHHA-S/Fe nanofibrous hydrogel, HHA-S was initially synthesized from HHA and 2-(methylthio) ethylamine via a condensation reaction. A new FTIR peak at 690 cm^{-1} corresponding to the C–S stretching vibration appears for HHA-S compared with HHA (Figure S1, Supporting Information). The successful conjugation of thioether groups on the side-chains of HHA was further confirmed by ^{1}H NMR and elemental analysis (Figure S2, Supporting Information). The sulfur content in HHA-S was 1.55 wt% with around 20% grafting ratio of thioether groups (molar percentage) (Table S1 and Figure S3, Supporting Information). Subsequently, HHA-S was electrospun to prepare nanofibers, FHHA-S, which were further crosslinked by Fe^{3+}.[16] In the FTIR spectrum of FHHA-S/Fe, appearance of a new peak at 1728 cm^{-1} indicates the coordination bond formation between Fe^{3+} and the carboxyl groups of HHA (Figure S4, Supporting Information), indicating the Fe^{3+} crosslinking. For comparison, FHHA and FHHA/Fe without thioether groups were also prepared. The morphology and elemental contents of the four nanofibers were observed and detected by SEM and ICP-MS, respectively. All nanofibers had uniform diameter distributions (**Figure 1**A). The mean diameters of nanofibers before and after Fe^{3+} crosslinking remained the same (Figure S5, Supporting Information), and FHHA-S/Fe (60 ± 11 nm) showed a smaller diameter distribution than that of FHHA/Fe (80 ± 13 nm). Elemental mapping of FHHA-S/Fe by energy dispersion spectroscopy (EDS) shows a homogeneous distribution of S (pink) and Fe (yellow) with contents of 7.79 and 10.02 μg mg^{-1}, respectively (Table S2, Supporting Information).

The in vitro water absorbing capacity and gelling performance of the HHA-based nanofibers were evaluated first. As shown in Figure 1B, the crosslinked nanofibers, FHHA/Fe and FHHA-S/Fe, formed transparent hydrogels after absorbing saline with equilibrium swelling of ≈600%. SEM images showed that the nanofibers crisscrossed in the FHHA/Fe and FHHA-S/Fe nanofibrous hydrogels with an average aperture of about 46 μm. The storage modulus (G') of FHHA/Fe and FHHA-S/Fe after absorbing saline were higher than their respective loss modulus (G''), demonstrating the formation of true gels (Figure 1C). G' and G'' curves showed frequency dependence, and increased with increasing frequency. The in situ gelling performance

of different nanofibers on the wound bed was next evaluated. Crosslinking of Fe^{3+} significantly improved the stability of the nanofibers in the wound exudate environment (Figure 1D,E). The FHHA/Fe and FHHA-S/Fe were infiltrated by the wound exudate gradually to become nanofibrous hydrogels within 24 h, which were partially degraded at 48 h and completely absorbed within 72 h. The weight of FHHA/Fe and FHHA-S/Fe first increased to around 5.5-fold of the initial mass by absorbing wound exudate and then gradually decreased due to the degradation and absorption. In contrast, those formulations without Fe^{3+} crosslinking, FHHA and FHHA-S, degraded within 2 h on the wound beds. These results demonstrated that crosslinked nanofibers, FHHA/Fe and FHHA-S/Fe, can form absorbable nanofibrous hydrogels in situ after being applied as a dressing on wound bed with a complete absorption rate of 3 days, which matches the dressing change frequency in clinic for shallow chronic wounds in diabetes (usually 2–3 days). No additional removal procedure is needed for these absorbable nanofibrous hydrogels, thus avoiding secondary injury and improving ease of patient care. The degradation of the FHHA/Fe and FHHA-S/Fe nanofibrous hydrogels is attributed to the release of Fe^{3+}, which is the crosslinker of the nanofibers. As shown in Figure 1F, the Fe^{3+} release increased along with the swelling of the nanofibrous hydrogels, and almost all of the Fe^{3+} was released within 72 h. Bacterial infection often appears throughout the process of wound healing. The released Fe^{3+} rendered the FHHA-S/Fe nanofibrous hydrogel with acceptable antibacterial activity against both *Staphylococcus aureus* and *Escherichia coli* bacteria (Figure S6, Supporting Information). Furthermore, no dead cells were observed after co-culturing of FHHA-S/Fe with normal L929 fibroblasts, and the cell density was comparable to that of the blank control, demonstrating that neither the FHHA-S/Fe or the released Fe^{3+} are cytotoxic to normal tissues (Figures S7–S9, Supporting Information).

2.2. FHHA-S/Fe Nanofibrous Hydrogel Exhibited Intrinsic ROS Scavenging Capacity by Grafted Thioethers and Transformative Effect on Macrophage Phenotype from M1 to M2 by HHA

H_2O_2, a kind of endogenously produced ROS, is one of the most important oxidative agents in acute and chronic wounds, and can cause oxidative stress and aggravate inflammatory reactions.[17] Therefore, the in vitro oxidation resistance of HHA-S was investigated by an H_2O_2 assay kit. As shown in **Figure 2**A, HHA-S decreased the concentration of H_2O_2 significantly to only 29% of its original level in 6 min, while HHA consumed a relatively little amount of H_2O_2 (Figure S10, Supporting Information) ($p < 0.001$), showing the excellent antioxidant properties of the grafted thioether groups on HHA. In addition, the antioxidant mechanism of HHA-S was verified by X-ray photoelectron spectroscopy (XPS). After H_2O_2 treatment of HHA-S, the intensity of the binding energy peak of S(II) at 163.80 eV decreased, while new peaks with binding energies of S(IV) at 166.45 eV and S(VI) at 168.55 eV appeared (Figure 2B), indicating the partial oxidation of the thioethers to sulfoxide and sulfone groups. The oxidation of thioethers was further confirmed by the ^1H NMR spectrum of HHA-S with the appearance of new peaks in the range of 2.8–3.2 ppm after adding H_2O_2 (Figure 2C).[18] The in vitro antioxidant activity of FHHA-S/Fe was evaluated using L929 fibroblast cells stimulated by Rosup agent to achieve excessive intracellular ROS. Dichlorofluorescein-diacetate (DCFH-DA) is an ROS probe, which is non-fluorescent until oxidized by intracellular ROS. As shown in Figure 2D and Figure S11 (Supporting Information), the DCFH fluorescence intensity of FHHA-S/Fe and FHHA-S treated cells was significantly lower than that of FHHA ($p < 0.01$) and FHHA/Fe ($p < 0.001$) treated cells, suggesting that the grafted thioether groups on HHA endowed the nanofibers with the potential to scavenge intracellular ROS (Figure S12, Supporting Information). The result demonstrate that FHHA-S/Fe exhibit excellent antioxidant properties by simple chemical modification of biocompatible HHA with thioether groups without adding any additional antioxidants, thus reducing the potential toxicity.

HHA has been demonstrated to promote the transformation of macrophages from a pro-inflammatory M1 phenotype to a reparative M2 phenotype.[13] M1 and M2 phenotype macrophages express different characteristic surface protein markers, and the M1 phenotype can be induced via exposure to lipopolysaccharide (LPS).[19] Cells exposed to LPS alone acted as the negative control in these experiments, while other groups were subsequently treated with nanofibers post-LPS exposure. The transformation of macrophages promoted by FHHA-S/Fe in the cellular level was first evaluated by flow cytometry. As shown in Figure 2E, after LPS stimulation alone, the percentages of $CD206^-CD86^+$ (M1 phenotype) and $CD206^+CD86^-$ (M2 phenotype) macrophages were 25.7% and 1.09%, respectively. However, after subsequent HHA-based nanofibers treatment, the percentages of macrophages in the M1 phenotype decreased to 1.0–2.0% while M2 phenotype increased to 20–25%. The results demonstrated the effective ability of HHA-based nanofibers to promote the transformation of macrophages from the M1 into the M2 phenotype, which was unaffected by the electrospinning or crosslinking processes. Similar results were also observed by immunofluorescence staining (Figure S13, Supporting Information). Compared with LPS alone, strong fluorescence intensity of CD206 protein was observed for all four groups of raw macrophages treated with HHA-based nanofibers (Figure 2F). It should be noted that the percentages of M2 phenotype macrophages in FHHA-S and FHHA-S/Fe groups (24.6% and 23.5%, respectively) were higher than that of nanofibers without thioether groups (21.3% and 20.6%), demonstrating that the grafted thioether groups enhanced the transformation of macrophage phenotype by consuming the endogenous ROS thereby reducing the oxidative stress.

2.3. FHHA-S/Fe Nanofibrous Hydrogel Enhanced the Healing Effect on Acute Wound Model

The demonstrated intrinsic dual modulation mechanisms of FHHA-S/F on inflammation at the cellular level (including antioxidant properties and transformation of macrophage phenotype) would be beneficial for effective wound healing in vivo. Thus, acute trauma-derived cutaneous wounds, one of the most common and major wounds, were established in mice to evaluate the healing effect of FHHA-S/Fe in vivo. As shown in **Figure 3**A, FHHA/Fe and FHHA-S/Fe were applied to the full-thickness

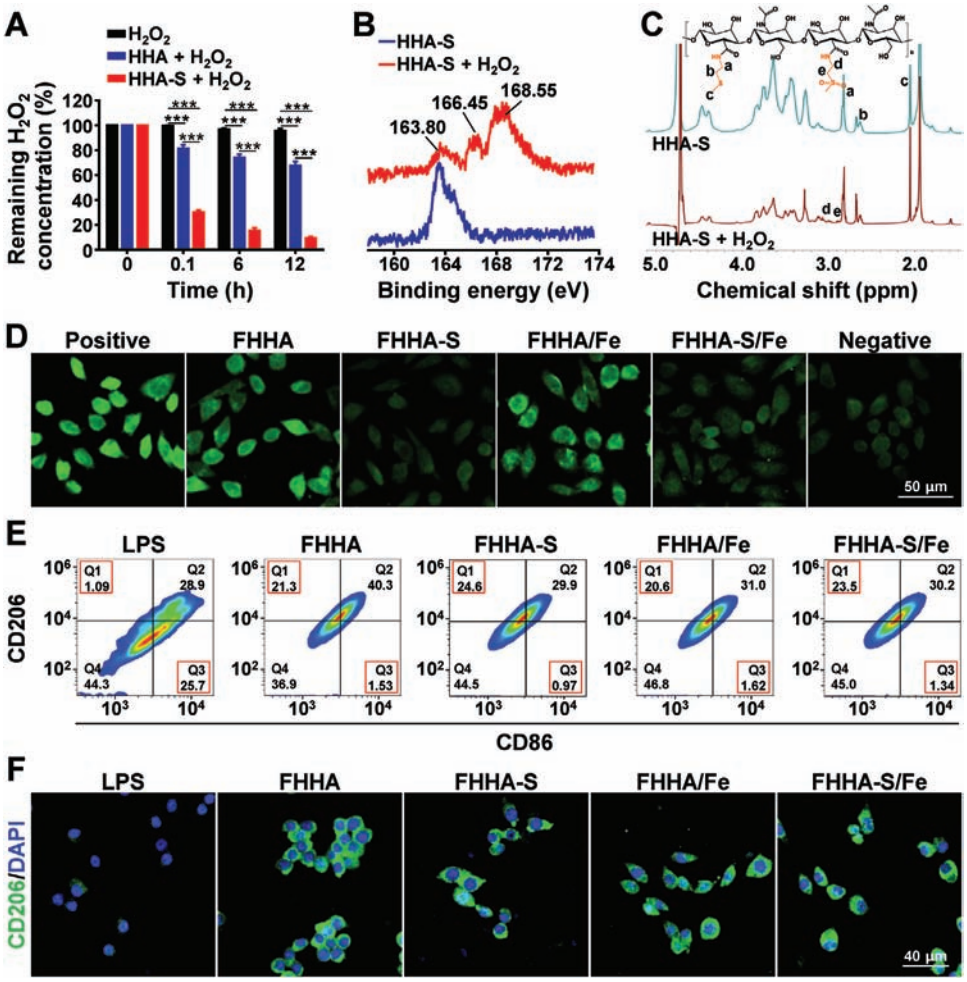

Figure 2. FHHA-S/Fe nanofibrous hydrogel exhibited intrinsic ROS scavenging capacity by grafted thioethers and transformative effect on macrophage phenotype from M1 to M2 by HHA. A) Remaining H_2O_2 concentration in comparison with the original H_2O_2 (10×10^{-6} M) after treatment with HHA or HHA-S at the indicated hours. ***$p < 0.001$, $n = 3$. B) XPS of sulfur of HHA-S before and after incubation with H_2O_2. C) ^{1}H NMR spectra of HHA-S before and after incubation with H_2O_2. D) CLSM images of Rosup-stimulated L929 cells after treatment with different nanofibers stained with DCFH-DA. Cells with only Rosup treatment were used as the positive control, and cells with no treatment were used as the negative control. E) Flow cytometry pattern of Raw 264.7 macrophages stained with CD206 and CD86 antibody after treatment with LPS and different nanofibers. F) CLSM images of Raw 264.7 macrophages stained with Hoechst (blue) and CD206 antibody (green) after treatment with LPS and different nanofibers.

acute wounds in Kunming mice. After applying dressing on the wound beds, FHHA/Fe and FHHA-S/Fe formed nanofibrous hydrogels quickly and were completely degraded and absorbed within 3 days to fit the targeted dressing change frequency (Figure 3B). According to the wound photos (Figure 3C) and closure curves (Figure 3D), the shrinkage of wound sizes in FHHA/Fe and FHHA-S/Fe groups were quicker than that of the control group, especially in the later treatment period. For instance, the average wound area after FHHA/Fe or FHHA-S/Fe treatments was around 25% at day 9, smaller than that of the control group (38.7%). Additionally, the average wound area of FHHA-S/Fe treatment further decreased to 3.6% at day 15, compared to 12.5% for FHHA/Fe treatment, indicating that the introduction of thioether groups in FHHA-S/Fe further promoted the wound regeneration in vivo. H&E staining of the wound tissue sections after treatment at day 15 were used to further evaluate the wound healing effect (Figure 3E). The thickest and most complete epidermis, and smallest wound gap were observed in FHHA-S/Fe group, while there were unhealed cavities beneath the epidermis in control group. Denser collagen deposition and a large amount of new vessels were also observed in FHHA-S/Fe group from Masson's trichrome stain (MTS) staining and CD31 (a vascular endothelial cell marker) immunofluorescence staining, respectively (Figures S14–S16, Supporting Information). However, the difference in wound healing speed of all the groups was not sufficiently significant, especially in the early wound regeneration stage before day 9. The average wound areas were very similar with and without dressing treatment at day 3 and day 6 (Figure 3D). For general acute wounds, the inflammation phase normally lasts for only 1–3 days.[4b,5d] Due to the fact that inflammatory responses in acute wounds on normal, wild type mice are not very strong, the transition of the wounds from the inflammation phase to the proliferation phase is relatively easy. So, the intrinsic dual modulation mechanisms of FHHA-S/F on the

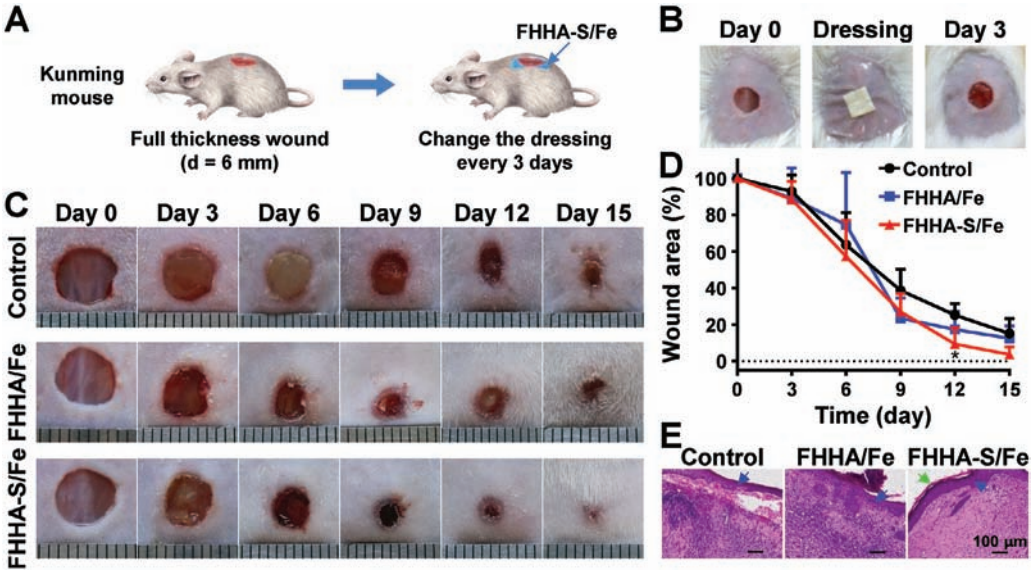

Figure 3. FHHA-S/Fe nanofibrous hydrogel enhanced the healing effect on acute wound model. A) The schematic establishment and treatment of an acute wound model. Saline given as control group, $n = 6$. B) Representative images of full thickness wound by 6-mm biopsy punch on the back of Kunming mouse at day 0, dressed by nanofibers and at day 3 with nanofibrous hydrogel treatment. C) Representative photographs of wounds after different treatments at indicated days. D) Quantitative analysis of wound area at the indicated days in comparison with the original wound. $n = 6$, $^*p < 0.05$ FHHA-S/Fe versus control. E) Representative images of wound tissues stained with H&E at day 15. Epidermis (blue) and stratum corneum (green) are marked by arrows.

inflammation microenvironment cannot be fully reflected in an acute wound model created on normal, wild type mice.

2.4. FHHA-S/Fe Nanofibrous Hydrogel Enhanced the Healing Effect on Chronic Diabetic Wound Model

For chronic wounds, the inflammation phase would be greatly extended or even unable to transition into the proliferation phase.[6] Hence, to further screen the wound healing efficacy of FHHA-S/Fe, a chronic diabetic wound model was established on C57BL/6 mice (**Figure 4**A). The mice were intraperitoneally injected by streptozotocin (STZ) for 5 days. When the blood glucose was sustained at over 11.1 mmol L^{-1} for 30 days, wounds were induced and the FHHA/Fe and FHHA-S/Fe wound dressings were administered.[20] Figure 4B shows the side-by-side comparison of the wounds in different groups on day 3, 6, 9, 12, and 15, respectively. According to the wound photos and closure curves (Figure 4C), FHHA/Fe and FHHA-S/Fe treatment led to a noticeable shrinkage in wound sizes, especially at the early wound regeneration stage, thus demonstrating the accelerated wound healing phase transition from inflammation to proliferation and remodeling. For the control group, the wound healing speed was rather slow in the first 9 days, the inflammatory period was prolonged, and abatement of the intense inflammatory response and the start of rapid proliferation did not occur until day 12. For instance, the average wound area of FHHA/Fe and FHHA-S/Fe groups was around 75% at day 3 and decreased to around 58% at day 6, much smaller than that of control group (85.1% and 83.9%, respectively). Interestingly, at day 9, the average wound area of FHHA-S/Fe group further decreased to 32.1%, while remaining at 50.1% for FHHA/Fe group and 75.4% for control group ($p < 0.05$), indicating that the introduction of thioether groups in FHHA-S/Fe further promoted the wound regeneration in vivo for the chronic wound model as well.

Histological examinations were carried out on day 15 to better evaluate the extent of wound healing. For H&E staining, the hair follicles, sebaceous glands, and squamous epithelium were all clearly observed in FHHA-S/Fe group, as would be observed in normal skin tissues. However, no hair follicles were found in the FHHA/Fe group and control group in the center of the wound beds, indicating less complete healing (Figure 4D). Collagen deposition is a critical factor to determine the strength and appearance of the skin and thus was evaluated using MTS staining.[7b] As shown in Figure 4E, there were pronounced differences in collagen deposition between all three groups as evidenced by the blue MTS staining intensity and area (Figure S17, Supporting Information). Among them, collagen deposition for the FHHA-S/Fe group was clearly the densest. In addition, the new vessels at the wound site were stained by CD31. Compared with the other treatment groups, many more new vessels were generated in the FHHA-S/Fe group (Figure 4F). CD31 fluorescence intensity per unit wound area of FHHA-S/Fe group was 3.3-fold and 1.5-fold higher than that of the control group ($p < 0.001$) and the FHHA/Fe group ($p < 0.01$), respectively (Figure 4G). The new vessels provide nutrients and oxygen to the metabolically active wound bed to promote the formation of granulation tissue (Figure S18, Supporting Information).[21] The evidences suggested that the FHHA-S/Fe enhanced healing efficacy of chronic diabetic wounds, accelerated granulation tissue formation and collagen deposition, and promoted neovascularization.

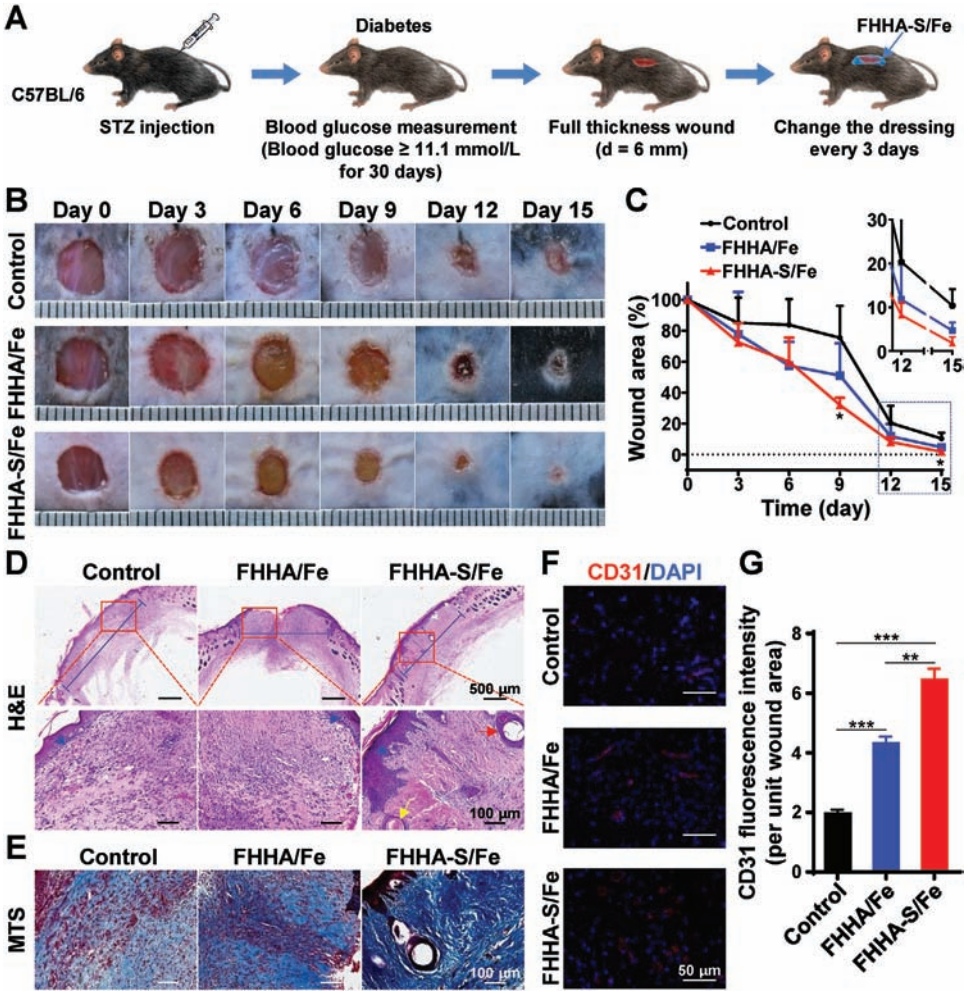

Figure 4. FHHA-S/Fe nanofibrous hydrogel enhanced the healing effect on a chronic diabetic wound model. A) Schematic of the establishment and treatment of a chronic diabetic wound model. Saline given as control group, $n = 6$. B) Representative photographs of wounds at indicated days with nanofibrous hydrogel treatment. C) Quantitative analysis of wound area at the indicated days in comparison with the original wound. $n = 6$, $^{*}p < 0.05$ FHHA-S/Fe versus control. D) Representative images of wound tissues stained with H&E at day 15. Wound gap, the distance between the advancing edges of wounds, is marked by a blue line. Epidermis (blue), hair follicles (red) and sebaceous gland (yellow) are marked by arrows. E) Representative images of wound tissues stained with MTS at day 15. F) Fluorescence images of new blood vessels in wound tissues stained with CD31 (red) at day 15. Nuclei were counterstained with DAPI (blue). G) Corresponding CD31 fluorescence intensity per unit wound area at day 15. $n = 6$, $^{***}p < 0.001$.

2.5. FHHA-S/Fe Nanofibrous Hydrogel Accelerated the Chronic Diabetic Wound Healing Phase Transition from Inflammation to Proliferation and Remodeling by Synergistic Modulation of Inflammation Microenvironment

Chronic diabetic wounds stay in the inflammation phase for an extended period due to the presence of a large number of ROS, M1 phenotype macrophages, and pro-inflammatory chemokines.[5] Therefore, to explore the mechanisms by which FHHA-S/Fe synergistically modulates the inflammation microenvironment, the wound tissues after different treatments were harvested on day 3 in the inflammation phase (**Figure 5**A). First, the content of ROS in the wound tissues was detected by immunofluorescence staining. Expression level of 3-nitrotyrosine protein is elevated in the presence of excessive ROS.[5a] As shown in Figure 5B, after FHHA-S/Fe treatment, the number of 3-nitrotyrosine-positive cells in the wound tissues was significantly lower than that of the control and FHHA/Fe groups (Figure S19, Supporting Information) ($p < 0.001$). A similar result was also observed when evaluating the expression level of 3-nitrotyrosine protein by western blotting (Figure S20, Supporting Information). The results indicated that FHHA-S/Fe could effectively scavenge ROS by grafted thioether groups. Subsequently, the macrophage phenotypes in the wound tissues were analyzed by immunofluorescence staining. As shown in Figure 5C, while most macrophages in the control group stayed in M1 phenotype ($F4/80^{+}CD206^{-}$), the wound tissues contained a large number of M2 phenotype macrophages ($F4/80^{+}CD206^{+}$) after FHHA-S/Fe and FHHA/Fe treatment, indicating that HHA-based nanofibers promoted the transformation of macrophages from a pro-inflammatory M1 to a reparative M2 phenotype in vivo. The numbers of different phenotype macrophages in the wound tissues were then quantified by flow cytometry (Figure 5D). Compared to the control group, the percentage of

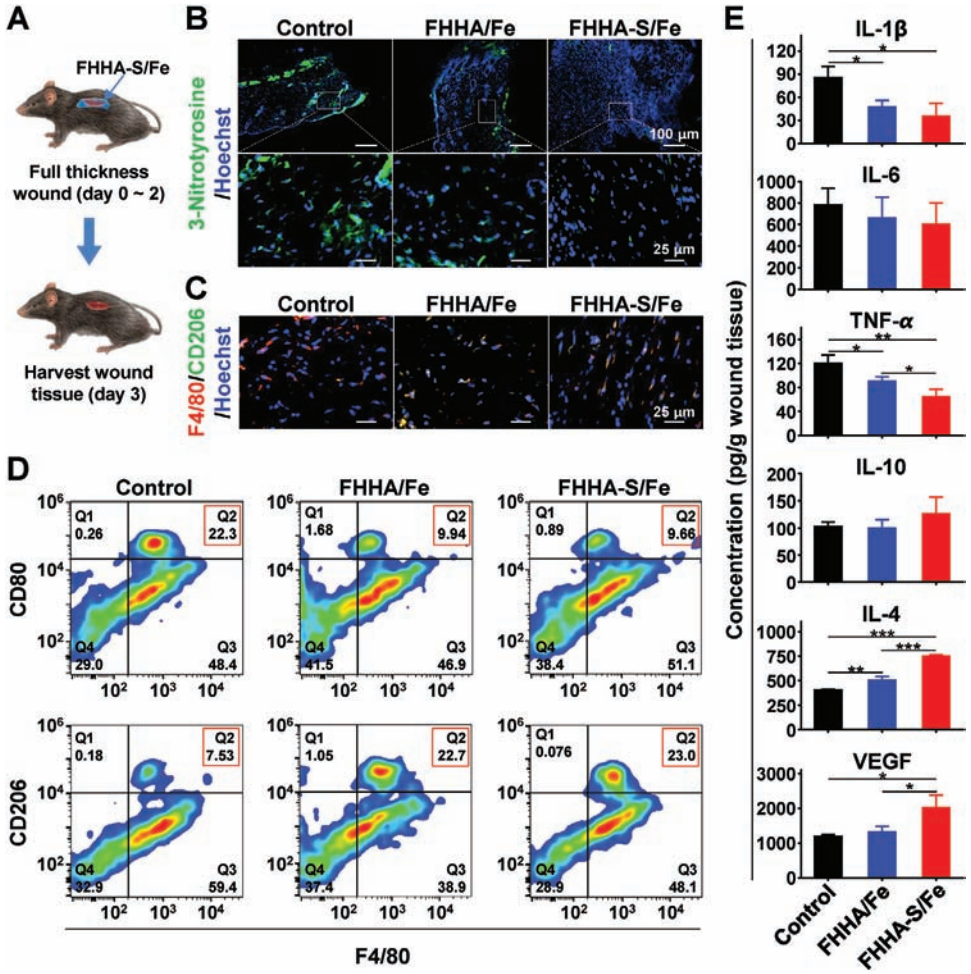

Figure 5. FHHA-S/Fe nanofibrous hydrogel accelerated the chronic diabetic wound healing phase transition from inflammation to proliferation and remodeling by synergistic modulation of inflammation microenvironment. A) Wound tissues were harvested at day 3 after different treatment for the following tests. Saline given as control group, $n = 3$. B) Immunofluorescence images of wound tissues after different treatment stained with 3-Nitrotyrosine (green). Nuclei were counterstained with Hoechst (blue). C) Immunofluorescence images of macrophages in wound tissues after different nanofibers treatment stained with F4/80 (red) and CD206 (green). Nuclei were counterstained with Hoechst (blue). D) Flow cytometry pattern of wound tissue cells stained with F4/80 and CD80 antibody or F4/80 and CD206 antibody after different nanofibers treatment. E) Chemokine concentrations in wound tissues were determined by ELISA. $n = 3$, $^{*}p < 0.05$, $^{**}p < 0.01$, $^{***}p < 0.001$.

$F4/80^{+}CD80^{+}$ macrophages (M1 phenotype) decreased from 22.3% to 9.94% and 9.66% after FHHA/Fe and FHHA-S/Fe treatment, respectively. In contrast, the percentages of M2 phenotype macrophages after FHHA/Fe and FHHA-S/Fe treatment (22.7% and 23.0%, respectively) were over threefold higher than that of the control group (7.53%), in agreement with the immunofluorescence staining result. Together, the results indicated that for chronic diabetic wounds, FHHA-S/Fe could scavenge ROS by grafted thioether groups to alleviate inflammatory reactions in the early wound healing stage, and promote the transformation of macrophages from pro-inflammatory M1 to reparative M2 phenotype through HHA in vivo, which accelerated the wound phase transition from inflammation to proliferation for enhanced healing effect.

To further confirm the effective wound phase transition after FHHA-S/Fe treatment, the contents of chemokines in wound tissues were detected by ELISA assays (Figure 5E). Compared with the control group, the contents of pro-inflammatory chemokines including interleukin-1beta (IL-1β), interleukin-6 (IL-6), and tumor necrosis factor alpha (TNF-α) were much lower in the FHHA-S/Fe and FHHA/Fe groups, suggesting that the inflammatory response was reduced in nanofibers groups. The difference in IL-1β content was significant (85.4 pg g^{-1} for control group, 47.3 pg g^{-1} for FHHA/Fe group and 35.3 pg g^{-1} for FHHA-S/Fe group) ($p < 0.05$). Similarly, the reduction in TNF-α compared to control was significant for the FHHA/Fe and FHHA-S/Fe groups ($p < 0.05$ and $p < 0.01$, respectively). It should be noted that the content of TNF-α in FHHA-S/Fe group was two thirds of that seen for FHHA/Fe group ($p < 0.05$), verifying that the effective scavenging of ROS contributed to the accelerated phase transition after FHHA-S/Fe treatment. The accelerated transition from inflammation phase to proliferation phase of the chronic diabetic wound after FHHA-S/Fe treatment may also promote the dissemination of anti-inflammatory cytokines,

such as interleukin-4 (IL-4) and interleukin-10 (IL-10). These anti-inflammatory cytokines contribute to the direct recruitment of M2 phenotype macrophages from surrounding tissues.[5d,22] For instance, the contents of IL-4 and IL-10 in FHHA-S/Fe group (750.4 and 126.3 pg g^{-1}, respectively) were higher than that of FHHA/Fe group (IL-4 505.6 pg g^{-1} ($p < 0.001$) and IL-10 99.8 pg g^{-1}, respectively). In addition, the M2 phenotype macrophages, which were transformed and recruited, can further secrete growth factors such as vascular endothelial growth factor (VEGF) for neovascularization. As expected, the content of VEGF protein in FHHA-S/Fe group was about 1.7-fold and 1.5-fold higher than that of control group and FHHA/Fe group, respectively ($p < 0.05$). This provides a nice mechanism for the distinct differences seen compared to the control group in the CD31 vascularization assay. Overall, the results indicated that FHHA-S/Fe could synergistically accelerate the wound phase transition from inflammation to proliferation, which keeps the diabetic chronic wounds in steady state of remodeling with enhanced healing effect.

3. Conclusion

In summary, we have reported an absorbable FHHA-S/Fe nanofibrous hydrogel with synergistic modulation mechanisms of the wound inflammation microenvironment to accelerate the healing phase transition from inflammation to proliferation and remodeling. The hydrogel can be completely degraded and absorbed within 3 days to fit the typical dressing change frequency of chronic diabetic wounds, thus enables avoidance of secondary injury. More importantly, the FHHA-S/Fe nanofibrous hydrogel exhibited intrinsic dual modulation mechanisms of inflammation including antioxidant properties and the capability of transforming the macrophage phenotype. Through the synergistic modulation of the inflammation microenvironment, the FHHA-S/Fe nanofibrous hydrogel resulted in accelerated wound healing in vivo especially on a chronic diabetic wound model. Overall, our results provide a simple and synergistic dressing strategy to improve healing efficacy for chronic wounds, which presents a new possibility for effective and safer wound management.

4. Experimental Section

Materials: High molecular weight hyaluronic acid (HHA, 1400 kDa, 97%) was purchased from Bloomage Freda Biopharm Co., Ltd. 2-(methylthio) ethylamine (97%), 1-ethyl-3-[3-dimethylaminopropyl] carbodiimide hydrochloride (EDC•HCl, 98%), and Na_2S (99%) were purchased from Changchun Third Party Pharmaceutical Technology Co., Ltd. 1-Hydroxybenzotriazole monohydrate (HOBt, 97%), $FeCl_3$•$6H_2O$ (AR), sodium citrate (99%), citric acid monohydrate, and agar were purchased from Aldrich Chemical Co., Ltd. Streptozotocin (STZ, 98%) was purchased from Shanghai Macklin Biochemical Co., Ltd. 25% ammonia water (AW) and *N*-methylopirolidone (NMP) was purchased from Beijing Chemical Works Co., Ltd..

Dulbeccos modified eagle medium (DMEM) and fetal bovine serum (FBS) were purchased from ThermoFisher Scientific. Hoechst 33 258 and 3-(4, 5-dimethylthiazol-2-yl)-2, 5-diphenyltetrazolium bromide (MTT) were bought from Sigma-Aldrich. Lipopolysaccharide (LPS), hematoxylin and eosin (H&E) and Masson's trichrome stain (MTS) kits were purchased from Beijing Solarbio Science & Technology Co., Ltd. Reactive oxygen species assay kit, hydrogen peroxide assay kit, enhanced bicinchoninic acid (BCA) protein assay kit, enhanced electrochemiluminescence (ECL) western blotting detection reagents, and mouse ELISA kits were purchased from Beyotime Biotechnology, China. Rabbit anti-CD31, rabbit anti-macrophage mannose receptor 1 antibody (CD206), rabbit anti-EMR1/F4/80/APC, rabbit anti-CD206/FITC, rabbit anti-CD86/APC, rabbit anti-CD80/FITC, and goat anti-rabbit IgG/FITC secondary antibody were purchased from Bioss Biotechnology Co., Ltd., Beijing, China. Cell counting kit-8 (CCK-8) was purchased from Dojindo. Calcein AM, propidium iodide was purchased from Nanjing KeyGen Biotech. Co. Ltd., China. Tegaderm transparent dressing was purchased from 3M Health Care.

Measurements: Nanofibers were prepared using electrospinning machines (TL-Pro, Shanghai, China). Fourier Transform Infrared (FTIR) measurements of HHA-S and nanofibers were carried out on a Bruker Vertex70 Win-IR instrument in the region of 400–4000 cm^{-1}. ^{1}H-NMR spectra of HHA-S before and after being oxidized were recorded on a Bruker AVANCE DRX 400 spectrometer using D_2O as the solvent at room temperature. Elemental content of HHA-S and elemental mapping of S and Fe in nanofibers were obtained by energy dispersion spectroscopy (EDS, OXFORD INSTRUMENTS X-MAX). Elemental analysis was carried out using an elemental analyzer (Vario EL cube, Elementar, Germany). The morphology of the nanofibers was observed using an environmental scanning electron microscope (SEM, XL-30 ESEM FEG Scanning Electron Microscope FEI COMPANYTM) at an acceleration voltage of 15 kV. ImageJ was used to analyze SEM images. The storage modulus (G') and loss modulus (G'') of nanofibrous hydrogels was measured on an AR2000 rheometer (TA Instruments) over a radian frequency range of 0.1–100 rad s^{-1} at 37 °C. Quantitative analysis of elemental sulfur and iron content was conducted using inductively coupled plasma mass spectrometry (ICP-MS, Xseries II, Thermoscientific, USA). The electron binding energy of sulfur in the thioether-grafted HHA (HHA-S) before and after being oxidized was identified by X-ray photoelectron spectroscopy (XPS) (Thermo ESCALAB 250). In vitro cellular fluorescence imaging was observed on a confocal laser scanning microscope (CLSM) imaging system (Zeiss710, Japan). Western blotting gels were detected using a Tanon 5200 Imager. Histological sections were observed on a BioTek Cytation5. Blood glucose was measured by glucometer (one touch Ultra easy, Johnson&Johnson).

Preparation of HHA-S: Briefly, HHA (100 mg) was dissolved in deionized water at a concentration of 2 mg mL^{-1}. EDC•HCl (145 mg) and 2-(methylthio) ethylamine (32 mg) were added to the solution. HOBt (76 mg) dissolved in dimethylsulfoxide (DMSO)/H_2O (1:1, 4 mL) was added to the reaction mixture. After mixing, the pH of the reaction mixture was adjusted to 6.8 with NaOH (0.1 mol L^{-1}) and HCl (0.1 mol L^{-1}) and the mixture was stirred in an ice bath for half an hour. Then the reaction mixture was stirred at room temperature for 3 days. Then, the reaction solution was precipitated in ice-cold ethanol. The precipitate was redissolved in distilled water and dialyzed. The purified product was freeze-dried.[23]

Preparation of FHHA-S: Electrostatic spinning solution of FHHA-S was prepared by dissolving HHA (15 mg) and HHA-S (15 mg) in a solution consisting of 25% AW (1.8 mL) and NMP (0.6 mL).[24] The polymer stream was fed through a needle of 0.6 mm diameter at a flow rate of 1 mL h^{-1}. The collector was kept 15 cm apart from the needle tip. The voltage at the collector and the nozzle were −2 and 20 kV, respectively. The process was carried out at 30 °C and 30% relative humidity.

Preparation of FHHA-S/Fe: Crosslinked nanofibers were prepared by the solution immersion method.[16] Briefly, FHHA and FHHA-S were immersed in anhydrous ethanol solution of $FeCl_3$•$6H_2O$ (5 mg mL^{-1}) for 24 h to obtain FHHA/Fe and FHHA-S/Fe, respectively. The nanofibers were washed three times with anhydrous ethanol for 30 min every time to remove noncrosslinked Fe^{3+} ions, and vacuum dried for 24 h to obtain the ionically crosslinked nanofibers.

Water Absorption Test: Water absorption of different nanofibers was measured by the gravimetric method. The nanofibers were cut into squares and weighed (m_1), and then soaked in saline. After the nanofibers fully

absorb saline, the nanofibers were weighed again (m_2), and the water absorption rate of the nanofibers was calculated according to the following equation

$$\text{Water absorption rate}\quad (\%) = \frac{m_2 - m_1}{m_1} \times 100\% \tag{1}$$

The nanofibers after absorbing saline were freeze-dried and their microstructures were characterized by SEM.

In Vitro Fe^{3+} Release: Release profiles of Fe from FHHA/Fe and FHHA-S/Fe were detected by transwell assay. Nanofibers were put in the inner transwell chambers and 1 mL of phosphate buffered saline (PBS, pH = 7.4) was added in the outer transwell chambers. The liquid level of PBS was 5 mm higher than the upper surface of the fibers. The transwell chambers were kept in a thermostable incubator at 37 °C with general shaking. At the pre-set interval, the release medium outside the transwell chambers (200 µL) was collected and replaced with the same volume of fresh solution. The Fe content was quantified by ICP-MS.

Cell Culture: A mouse fibroblast cell line (L929) and a mouse macrophage cell line (Raw 264.7) were used in this study. These cell lines were cultured in DMEM supplemented with 10% FBS, penicillin (60 mg mL^{-1}) and streptomycin (100 mg mL^{-1}) under the condition of 37 °C, 5% CO_2.

In Vitro Scavenging of Hydrogen Peroxide (H_2O_2): The H_2O_2 scavenging abilities of HHA-S and FHHA-S were detected using an H_2O_2 assay kit with slightly different protocols. Briefly, the HHA-S was dissolved in distilled water at a concentration of 5 mg mL^{-1}. H_2O_2 (2 µL, 10 mmol L^{-1}) solution was added to the above solution (2 mL). For the FHHA-S, a piece of FHHA-S (10 mg) was instead directly added to the H_2O_2 (2 mL, 10 µmol L^{-1}) solution. All above solutions were placed at 37 °C. At appropriate time intervals, the H_2O_2 concentrations of the solutions were determined according to the manufacturer's protocol.

Scavenging of Intracellular ROS: The intracellular ROS scavenging ability of HHA-S and nanofibers was measured by ROS assay kit.[25] L929 cells (5×10^5 cells per well) were seeded in 6-well plates and incubated for 24 h. Cells were treated with Rosup (2 mL, 1 µg mL^{-1}) for 7 h. Then the cells were treated with DMEM (10% FBS) solutions containing HHA-S (5 or 7 mg mL^{-1}) and Rosup (1 µg mL^{-1}) or treated with a piece of nanofibers (5 mg) for 12 h, respectively. Cells with only Rosup treatment were used as the positive control, and cells with no treatment were used as the negative control. The culture medium was removed and dichlorofluorescein-diacetate (DCFH-DA, 1 mL, 1 µL mL^{-1}) in serum-free medium was added to each well. After incubation for 20 min, the cells were imaged by CLSM.

Effect of HHA-S and Nanofibers on Macrophage Phenotypes: Raw 264.7 cells (1×10^5 cells per well) were cultured on sterilized glass coverslips placed in a 24-well plate. After 24 h incubation, LPS in serum-free medium at a final concentration of 1 µg mL^{-1} was added, and the cells were cultured for another 12 h. The LPS solution was removed and then cells were treated with DMEM (10% FBS) solutions containing HHA-S at a concentration of 5 mg mL^{-1} or DMEM (1 mL, 10% FBS) with a piece of nanofibers (5 mg) for 12 h. Cells treated with LPS alone were used as the negative control. The glass coverslips were washed thrice with PBS. Next, the coverslips were fixed by 4% paraformaldehyde for 20 min and then were blocked with 1% bovine serum albumin for 1.5 h. After that, the coverslips were incubated in sequence with primary antibodies CD206 at 4 °C overnight, secondary antibodies for 1.5 h at room temperature and Hoechst 33 258 for 8 min in the dark. Then, the coverslips were mounted on glass slides with glycerin jelly, sealed with clear nail polish, and imaged by CLSM. The effect of nanofibers on macrophage phenotypes was also detected by flow cytometry. Raw 264.7 (4×10^5 cells per well) were cultured in a 6-well plate. After treatment with LPS and nanofibers as described above, the cells were collected by trypsin treatment and then were incubated with 5% BSA containing the rabbit anti-CD206/FITC antibody and rabbit anti-CD86/APC antibody for 1 h at 37 °C for flow cytometry detection.

Animal Used: Male Kunming mice and male C57BL/6 mice (20–25 g) were purchased from Beijing Huafukang Biological Technology Co., Ltd. Animal studies were approved by Ethical Committee of Changchun Institute of Applied Chemistry, Chinese Academy of Sciences. For induction of type 1 diabetes, C57BL/6 mice fasted for 12 h were injected with STZ dissolved in sterile citrate buffer (0.05 mol L^{-1} sodium citrate, pH 4.5, 70 mg kg^{-1}). STZ was administered continuously for 5 days. Then blood glucose was measured every 3 days. When blood glucose remained above 11.1 mmol L^{-1} for 30 days, the diabetes model was successfully established.[20]

In Vivo Absorption Ability of Nanofibers: Kunming mice were anesthetized by an intraperitoneal injection of 1% sodium pentobarbital (n = 3). Four full-thickness wounds were inflicted with 6 mm biopsy punches on the shaved back. The created wounds were covered by different nanofibers with the same size respectively. At pre-set interval, wound sites and nanofibers were photographed. The weight of nanofibers was recorded.

In Vivo Wound Healing Experiments: Wild Kunming mice and diabetic C57BL/6 mice were used in acute and chronic wound healing test, respectively. The mice were randomly divided into 3 groups (n = 6). All the animals were anesthetized by an intraperitoneal injection of 1% sodium pentobarbital, and the dorsal area was shaved and depilated with 8% Na_2S. Full-thickness wounds were inflicted with 6 mm biopsy punches on the shaved back. FHHA-S and FHHA-S/Fe were applied to the wounds, with saline as the control group. Tegaderm transparent dressing was administered as the secondary dressing to keep the nanofibers in place. At day 0, 3, 6, 9, 12, and 15 post-wounding, wound sites were photographed. Wound areas in each group were measured using the ImageJ software. The percent of wound area at the indicated days in comparison with the original wound was calculated according to the equation as below

$$\text{Wound area}_{\text{day\#}}\quad (\%) = \frac{\text{Wound area}_{\text{day\#}}}{\text{Wound area}_{\text{day0}}} \times 100\% \tag{2}$$

$\text{Wound area}_{\text{day\#}}$ and $\text{Wound area}_{\text{day0}}$ are the wound area after treatment at day # and day 0, respectively.

Histological Analysis: At day 15 after the operation, animals were sacrificed and tissue samples including the wound area and the surrounding skin were excised. For histological studies, the skin was fixed in 4% paraformaldehyde in PBS (0.01 M, pH = 7.4) overnight and embedded in paraffin. The tissue samples were sliced into sections of 4 µm thickness and stained with H&E, MTS and CD31 immunofluorescence staining. The stained sections were analyzed, and the images were captured using a BioTek Cytation5.

Quantitative Analysis of Proteins: For diabetes C57BL/6 mice, 3 days after the operation, mice were sacrificed (n = 3). Tissue samples including the wound area and the surrounding skin were excised and divided into two factions. One faction of tissue samples was used for immunofluorescence section to study tissue expression of F4/80, CD206, and 3-Nitrotyrosine. For the other faction, the proteins were isolated from the tissue samples and quantified by ELISA (IL-1β, IL-6, TNF-α, IL-4, IL-10, and VEGF) and Western Blotting (3-Nitrotyrosine).

Flow Cytometry: For the analysis of macrophages at the wound site of diabetes C57BL/6 mice, tissue samples including the wound area and the surrounding skin were harvested at day 3 after the operation (n = 3). Cells were isolated from the tissue samples and stained with rabbit anti-EMR1/F4/80/APC and rabbit anti-CD206/FITC or rabbit anti-EMR1/F4/80/APC and rabbit anti-CD80/FITC for flow cytometry detection.

Statistical Analysis: The statistical difference between groups was carried out by a paired Student's t-test using Origin software and p value < 0.05 was considered statistically significant. Acute and chronic wound healing experiments had six replicates (n = 6), and the other experiments had three replicates (n = 3). Data were presented as mean ± standard deviation (SD).

Supporting Information

Supporting Information is available from the Wiley Online Library or from the author.

Acknowledgements

The authors acknowledge the financial support from National Natural Science Foundation of China (Grant Nos. 51673188, 51773198, and 21975246). The authors would like to thank Zachary Schneiderman (Johns Hopkins University) for proofreading the manuscript. The animal studies were approved by the local institution review board and performed according to the Guidelines of the Committee on Animal Use and Care of Chinese Academy of Sciences.

Conflict of Interest

The authors declare no conflict of interest.

Keywords

absorbable dressings, diabetes, inflammation microenvironments, nanofibrous hydrogels, wound healing

Received: February 7, 2020
Revised: March 26, 2020
Published online:

[1] a) X. G. Liu, D. L. Huang, C. Lai, L. Qin, G. M. Zeng, P. Xu, B. S. Li, H. Yi, M. M. Zhang, *Small* **2019**, *15*, 1900133; b) N. H. Cho, J. E. Shaw, S. Karuranga, Y. Huang, J. D. D. Fernandes, A. W. Ohlrogge, B. Malanda, *Diabetes Res. Clin. Pract.* **2018**, *138*, 271.

[2] a) W. J. Jeffcoate, K. G. Harding, *Lancet* **2003**, *361*, 1545; b) Y. W. Kwon, S. C. Heo, T. W. Lee, G. T. Park, J. W. Yoon, I. H. Jang, S. C. Kim, H. C. Ko, Y. Ryu, H. Kang, C. M. Ha, S. C. Lee, J. H. Kim, *Sci. Rep.* **2017**, *7*, 1.

[3] a) J. L. Harding, M. E. Pavkov, E. W. Gregg, N. R. Burrows, *Diabetes Care* **2019**, *42*, 1430; b) H. Kampfer, R. Schmidt, G. Geisslinger, J. Pfeilschifter, S. Frank, *Diabetes* **2005**, *54*, 1543.

[4] a) A. J. Singer, R. A. F. Clark, *N. Engl. J. Med.* **1999**, *341*, 738; b) M. A. M. Jahromi, P. S. Zangabad, S. M. M. Basri, K. S. Zangabad, A. Ghamarypour, A. R. Aref, M. Karimi, M. R. Hamblin, *Adv. Drug Delivery Rev.* **2018**, *123*, 33.

[5] a) M. Schafer, S. Werner, *Pharmacol. Res.* **2008**, *58*, 165; b) S. Selvaraj, N. N. Fathima, *ACS Appl. Mater. Interfaces* **2017**, *9*, 5916; c) N. Lohmann, L. Schirmer, P. Atallah, E. Wandel, R. A. Ferrer, C. Werner, J. C. Simon, S. Franz, U. Freudenberg, *Sci. Transl. Med.* **2017**, *9*, eaai9044; d) N. X. Landen, D. Q. Li, M. Stahle, *Cell. Mol. Life Sci.* **2016**, *73*, 3861; e) J. H. Wang, X. Y. Chen, Y. Zhao, Y. M. Yang, W. J. Wang, C. Wu, B. Z. Yang, Z. T. Zhang, L. S. Zhang, Y. Liu, X. C. Du, W. F. Li, L. Qiu, P. J. Jiang, X. Z. Mou, Y. Q. Li, *ACS Nano* **2019**, *13*, 11686.

[6] A. Sindrilaru, T. Peters, S. Wieschalka, C. Baican, A. Baican, H. Peter, A. Hainzl, S. Schatz, Y. Qi, A. Schlecht, J. M. Weiss, M. Wlaschek, C. Sunderkotter, K. Scharffetter-Kochanek, *J. Clin. Invest.* **2011**, *121*, 985.

[7] a) G. P. Chen, Y. R. Yu, X. W. Wu, G. F. Wang, J. N. Ren, Y. J. Zhao, *Adv. Funct. Mater.* **2018**, *28*, 1801386; b) J. Wu, J. J. Zhu, C. C. He, Z. C. Xiao, J. J. Ye, Y. Li, A. Q. Chen, H. Y. Zhang, X. K. Li, L. Lin, Y. Z. Zhao, J. Zheng, J. Xiao, *ACS Appl. Mater. Interfaces* **2016**, *8*, 18710.

[8] a) Y. Yang, L. Ma, C. Cheng, Y. Y. Deng, J. B. Huang, X. Fan, C. X. Nie, W. F. Zhao, C. D. Zhao, *Adv. Funct. Mater.* **2018**, *28*, 1705708; b) X. Zhao, H. Wu, B. L. Guo, R. N. Dong, Y. S. Qiu, P. X. Ma, *Biomaterials* **2017**, *122*, 34; c) W. P. Li, C. H. Su, S. J. Wang, F. J. Tsai, C. T. Chang, M. C. Liao, C. C. Yu, T. T. V. Tran, C. N. Lee, W. T. Chiu, T. W. Wong, C. S. Yeh, *ACS Nano* **2017**, *11*, 5826.

[9] a) J. M. Kang, Z. Li, C. L. Organ, C. M. Park, C. T. Yang, A. Pacheco, D. F. Wang, D. J. Lefer, M. Xian, *J. Am. Chem. Soc.* **2016**, *138*, 6336; b) J. Wu, A. Q. Chen, Y. J. Zhou, S. Zheng, Y. Yang, Y. An, K. Xu, H. C. He, J. M. Kang, J. A. Luckanagul, M. Xian, J. Xiao, Q. Wang, *Biomaterials* **2019**, *222*, 119398; c) B. Saleh, H. K. Dhaliwal, R. Portillo-Lara, E. Shirzaei Sani, R. Abdi, M. M. Amiji, N. Annabi, *Small* **2019**, *15*, 1902232; d) X. R. Feng, W. G. Xu, Z. M. Li, W. T. Song, J. X. Ding, X. S. Chen, *Adv. Sci.* **2019**, *6*, 1900101.

[10] K. C. Broussard, J. G. Powers, *Am. J. Clin. Dermatol.* **2013**, *14*, 449.

[11] X. Y. Mao, R. Y. Cheng, H. B. Zhang, J. H. Bae, L. Y. Cheng, L. Zhang, L. F. Deng, W. G. Cui, Y. G. Zhang, H. A. Santos, X. M. Sun, *Adv. Sci.* **2019**, *6*, 1801555.

[12] a) X. Zhao, X. M. Sun, L. Yildirimer, Q. Lang, Z. Y. Lin, R. L. Zheng, Y. G. Zhang, W. G. Cui, N. Annabi, A. Khademhosseini, *Acta Biomater.* **2017**, *49*, 66; b) R. J. Wade, E. J. Bassin, W. M. Gramlich, J. A. Burdick, *Adv. Mater.* **2015**, *27*, 1356; c) F. Wang, W. Ji, P. Yang, C. -L. Feng, *ACS Nano* **2019**, *13*, 7281.

[13] a) L. D. Yu, P. Hu, Y. Chen, *Adv. Mater.* **2018**, *30*, 1801964; b) J. E. Rayahin, J. S. Buhrman, Y. Zhang, T. J. Koh, R. A. Gemeinhart, *ACS Biomater. Sci. Eng.* **2015**, *1*, 481; c) J. Wang, P. Kubes, *Cell* **2016**, *165*, 668; d) A. Boddupalli, L. D. Zhu, K. M. Bratlie, *Adv. Healthcare Mater.* **2016**, *5*, 2575.

[14] a) T. A. Wynn, K. M. Vannella, *Immunity* **2016**, *44*, 450; b) J. J. Gan, C. Y. Liu, H. L. Li, S. C. Wang, Z. Z. Wang, Z. Q. Kang, Z. Huang, J. F. Zhang, C. M. Wang, D. L. Lv, L. Dong, *Biomaterials* **2019**, *219*, 119340.

[15] a) B. R. Freedman, D. J. Mooney, *Adv. Mater.* **2019**, *31*, 1806695; b) R. Tian, X. Y. Qin, P. Y. Yuan, K. Lei, L. Wang, Y. K. Bai, S. Y. Liu, X. Chen, *ACS Appl. Mater. Interfaces* **2018**, *10*, 17018.

[16] C. L. Sheu, K. T. Shalumon, C. H. Chen, C. Y. Kuo, Y. T. Fong, J. P. Chen, *J. Mater. Chem. B* **2016**, *4*, 6680.

[17] a) J. R. Burgoyne, S. Oka, N. Ale-Agha, P. Eaton, *Antioxid. Redox Signaling* **2013**, *18*, 1042; b) R. J. Toh, C. C. Mayorga-Martinez, Z. Sofer, M. Pumera, *Adv. Funct. Mater.* **2017**, *27*, 1604923.

[18] a) S. J. Yu, C. Wang, J. C. Yu, J. Q. Wang, Y. Lu, Y. Q. Zhang, X. D. Zhang, Q. Y. Hu, W. J. Sun, C. L. He, X. S. Chen, Z. Gu, *Adv. Mater.* **2018**, *30*, 1801527; b) Q. H. Xu, C. L. He, K. X. Ren, C. S. Xiao, X. S. Chen, *Adv. Healthcare Mater.* **2016**, *5*, 1979.

[19] a) P. K. Langston, A. Nambu, J. Jung, M. Shibata, H. I. Aksoylar, J. H. Lei, P. N. Xu, M. T. Doan, H. L. Jiang, M. R. MacArthur, X. Gao, Y. Kong, E. T. Chouchani, J. W. Locasale, N. W. Synder, T. Horng, *Nat. Immunol.* **2019**, *20*, 1186; b) T. H. Kim, M. S. Kang, N. Mandakhbayar, A. El-Fiqi, H. W. Kim, *Biomaterials* **2019**, *207*, 23.

[20] a) H. S. Ma, Q. Zhou, J. Chang, C. T. Wu, *ACS Nano* **2019**, *13*, 4302; b) H. Soleimani, A. Amini, S. Taheri, E. Sajadi, S. Shafikhani, L. A. Schuger, V. B. Reddy, S. K. Ghoreishi, R. Pouriran, S. Chien, M. Bayat, *J. Photochem. Photobiol., B* **2018**, *181*, 23.

[21] a) H. Chen, R. Y. Cheng, X. Zhao, Y. H. Zhang, A. Tam, Y. F. Yan, H. K. Shen, Y. S. Zhang, J. Qi, Y. Feng, L. Liu, G. Q. Pan, W. G. Cui, L. F. Deng, *NPG Asia Mater.* **2019**, *11*, 3; b) F. Arnold, D. C. West, *Pharmacol. Ther.* **1991**, *52*, 407.

[22] a) T. A. Wynn, A. Chawla, J. W. Pollard, *Nature* **2013**, *496*, 445; b) S. A. Eming, T. A. Wynn, P. Martin, *Science* **2017**, *356*, 1026.

[23] a) C. E. Schante, G. Zuber, C. Herlin, T. F. Vandamme, *Carbohydr. Polym.* **2011**, *85*, 469; b) P. Bulpitt, D. Aeschlimann, *J. Biomed. Mater. Res.* **1999**, *47*, 152.

[24] E. Pabjanczyk-Wlazlo, I. Krucinska, M. Chrzanowski, G. Szparaga, A. Chaberska, B. Kolesinska, A. Komisarczyk, M. Bogun, *Fibres Text. East. Eur.* **2017**, *25*, 45.

[25] Y. J. Wu, D. F. Zhou, Y. X. Qi, Z. G. Xie, X. S. Chen, X. B. Jing, Y. B. Huang, *RSC Adv.* **2015**, *5*, 31972.